

Research Article

Improvement of Photovoltaic Power Plant Energy and Harmonic Attenuation for Grid Enhancement

Kitmo^{1,*} , Deli Goron¹ , Bikai Jacques² , Colbert Bab é¹ , No ð Djongyang¹ 

¹Department of Renewable Energy, National Advanced School of Engineering of Maroua, University of Maroua, Maroua, Cameroon

²Department Energy Engineering, IUT of Ngaound é é Ngaound é é, Cameroon

Abstract

This article presents a method for power factor correction and power compensation taking into account the injection of distributed generators in the distribution networks. Distribution networks are most often exposed to problems of harmonic disturbance. This work proposes a method that combines active filters and perturb and observe algorithms to reduce the rate of harmonic distortion in a photovoltaic system that is to be fed into power grids. A THD of 2.14% is achieved in compliance with the IEEE 519-2014 standard. Voltage and current profiles have good waveforms. The voltage level is regulated by the PI regulator. The perturb and observe algorithms associated with the filter developed in this work have shown their superiority in terms of voltage stability and power demand management for a grid-connected photovoltaic system.

Keywords

Harmonics Mitigation, Sustainable System, Optimal Power Generation, Power Quality Improvement, Photovoltaic Power Plant, On Grid

1. Introduction

Most countries around the world have understood the need to move away from energies whose production releases greenhouse gases [1]. As a result, many countries in Europe, Asia and Africa have embarked on the technology and development of renewable energies such as solar photovoltaic, wind power, biomass, geothermal and hydroelectric power. Cameroon, like other african countries in general and Central Africa in particular, has multiplied its use of renewable energy sources to meet the growing demand for electricity in its various localities, and to reinforce the power grids in urban areas [2]. These include photovoltaic solar power plants,

biomass power plants and hydroelectric power plants [3]. Most sources of electrical energy in Cameroon are hydroelectric power plants. These include the Song Loulou hydroelectric power station, the Lagdo hydroelectric power station and the Ed é hydroelectric power station [4]. In addition to these energy sources, there are also thermal power plants. Unfortunately, whatever thermal power plants are used in Cameroon, they are responsible for greenhouse gas emissions [5]. That's why many of today's conventions, such as the Convention on Climate Change, the Kyoto Protocol, impose an emission rate for greenhouse gases such as carbon dioxide,

*Corresponding author: kitmobahn@gmail.com (Kitmo)

Received: 17 May 2025; **Accepted:** 23 June 2025; **Published:** 15 July 2025



Copyright: © The Author(s), 2025. Published by Science Publishing Group. This is an **Open Access** article, distributed under the terms of the Creative Commons Attribution 4.0 License (<http://creativecommons.org/licenses/by/4.0/>), which permits unrestricted use, distribution and reproduction in any medium, provided the original work is properly cited.

sulfur or carbon monoxide. Power electronics are playing an increasingly important role in optimizing energy systems, with the aim of harnessing renewable energy sources. There has been a considerable evolution in the speed of power electronic switches, on the one hand, and in the choice of materials used in renewable energy production, on the other. Some energy sources, such as wind power plants, require a good knowledge of technology in order to be able to integrate them into primary sources such as hydroelectric or solar power plants [6].

Since the development of power electronics, most work over the last few decades has focused on developing algorithms for optimizing energy systems [7]. These include algorithms based on human behavior, or biologically inspired algorithms, or algorithms based on animal behavior. Among the most widely used algorithms for optimizing energy systems are particle swarm optimization [8], whale swarm optimization, mouse swarm optimization, lion troop optimization and gorilla troop optimization [9]. The best-performing algorithms are those with a fast convergence speed. The objective function defines the optimization criteria that enable reduced power loss and good voltage and current stability.

Although the world's population is growing every year, the use of fossil fuels is a danger to living beings on our planet. This consumption leads to atmospheric pollution, and even the depletion of these resources, making the price of oil unstable. This is why we are encouraged to limit greenhouse gas emissions, which is why we are interested in renewable energies [10]. The aim of this article is firstly to assess the availability of solar energy, and secondly to investigate methods for estimating global solar radiation [11]. There are several methods for estimating solar radiation on the inclined and horizontal planes. Some methods of estimating solar radiation or calibration are very costly [12]. However, the theoretical study of measurement data often presents certain inconsistencies, so in the work of [13], certain methods of evaluating solar radiation are proposed. A review of the literature in [14] also presents the most widely used methods for extrapolating solar irradiance on the horizontal plane. In [15], the method of extrapolating solar irradiance on the inclined plane is proposed [16]. Among the most widely used methods for estimating global solar radiation are real-time machine learning algorithms, the use of meteorological data and the exploitation of geographical information on study areas. In [17], a study is made of the evaluation of global solar radiation for the Maroua locality. This approach involved using and comparing empirical models with the results obtained. From this work, it was shown that it is during the dry season that the maximum values of photovoltaic solar power are produced. Voltage profiles on the IEEE 33 bus showed that power grids into which 50MW of power is injected are stable during the dry season. The study in [18] showed that the interconnected North Cameroon grids could be strengthened by the installation of a solar power plant in the Guider locality, which is why a photovoltaic power plant has been installed

there since 2022. In Cameroon's Far North region, a study has shown that only 30% of the population has access to electricity, in contrast to other regions of the country [19]. And yet, the Far North region has an abundance of photovoltaic solar energy. This is one of the regions where the literacy rate is too low, which justifies the fact that few people have access to electricity or a minimum level of comfort. However, the development of any country in the world inevitably requires access to drinking water and education. Every year, the cholera epidemic is detected because populations have no access to drinking water [20]. On the other hand, access to healthcare is becoming more and more difficult, as the energy to run biomedical equipment is non-existent. The only option the government offers the region is the use of thermal power plants, which provide intermittent, unstable electricity. Delays and untimely power cuts are recurrent [21]. These generators regularly break down. What's more, the diesel fuel used to run the thermal generators is very expensive and highly polluting. This is a major scourge that needs to be eradicated, as it hampers the country's socio-economic development and affects people's quality of life [22].

2. Methodology

Photovoltaic generators are powered by natural resources such as sunshine and temperature. These data need to be studied in order to validate the feasibility of a solar field. In this section, the proposed method uses Angstrom-Prescott extrapolation [23], which allows us to evaluate solar irradiance in the horizontal plane based on a succession of years. Equation (1) formalizes this extrapolation method. Equation 4 also contains the parameters required for the mathematical formulation of the photovoltaic system. Azimuth and tilt are also important factors in assessing the amount of sunshine in a given locality. Temperature is also an essential parameter in the study of a photovoltaic system, as a minimum temperature must be considered for extracting power from a photovoltaic array [24]. Under standard conditions, a temperature of 25 degrees allows maximum extraction of photovoltaic power. Meteorological data can often be used as an approximation [25]. These variables can be used to run a numerical simulation. The results section shows the power, current and voltage profiles obtained using this method.

The most practical correlation for assessing global solar radiation and the most commonly used is given by the relation [26]:

$$\frac{\xi}{\xi_0} = x + y \left(\frac{\phi}{\phi_0} \right) \quad (1)$$

Thus, by Equations (5), (6) and (7), the correlation parameters can be defined as:

$$x = -0.3012 + 0.4501 \cos \alpha + 0.323 \left(\frac{\phi}{\phi_0} \right) \quad (2)$$

$$y = 2.0212 - 0.1012 \cos \alpha - 0.694 \left(\frac{\phi}{\phi_0} \right) \quad (3)$$

Thus, the duration of sunshine is given by

$$\phi_0 = \frac{3}{41} \cos^{-1}(-\tan \gamma \tan \theta) \quad (4)$$

where ϕ_0 is monthly average day length (h); ϕ monthly average daily hours of bright sunshine (h) and x, y regression coefficients.

3. Modeling and Strategy of Filtering

The difficulty in using active or passive filters arises from the fact that some filters generate too much Joule effect loss and switching loss. Passive filters are sources of Joule effect losses. Active filters, on the other hand, increase harmonic distortion when the current draw of non-linear loads is high. However, the filter shown in Figure 1 has capacitors in each

switching cell and in each switching arm. The switches in the switching cells are complementary in pairs. Each arm has three communication cells made up of IGBT switches. This filter has the particularity of absorbing continuous quantities for short periods. This energy is then restored the next time the switches are switched or opened. In the absence of these capacitors, there will be a switching delay at the switches. Since capacitors are used to compensate for reactive energy and these filters do not contain any resistive components, the proposed model has the advantage of reducing losses due to Joule effects on the one hand and reducing the switching delay on the other. Most active filters do not allow the quantities of non-linear sources to be depolluted so as to comply adequately with the IEEE 519 standard [27].

The harmonics deform the signal waveforms, so after defining the photovoltaic power conversion stages, an active filter is placed downstream to clean the system of harmonics and inter-harmonics. Confirmation of the reduction in the rate of harmonic distortion is provided by the calculation of the rate of distortion defined in the IEEE 519 -2014 standard.

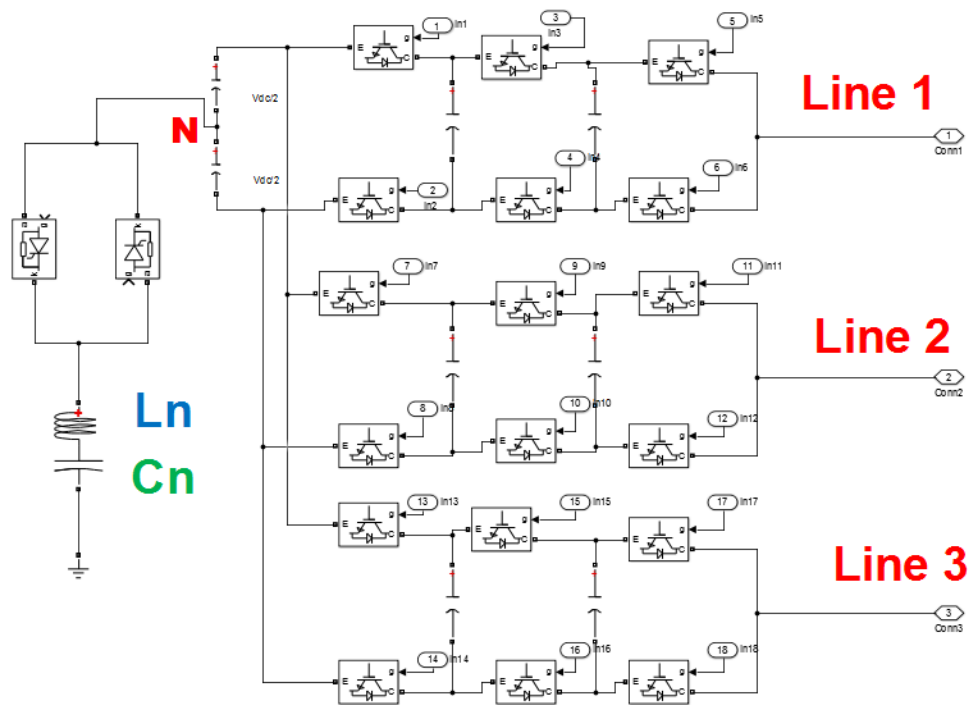


Figure 1. Model of proposed filter.

4. Boost Chopper

A static converter DC_DC has been used in this work. Its duty cycle is controlled by the MPPT controlled. Figure 2 is the boost chopper used for the system.

Photovoltaic energy is converted using a boost converter.

Controlling the duty cycle of this chopper enables maximum power to be extracted by MPPT control.

The chopper parameters in Figure 2 are defined by Equations (5) and (6). These equations define the correct operation of this conversion stage for maximum power extraction on the one hand, and for easy control of the duty cycle under optimal operating conditions on the other.

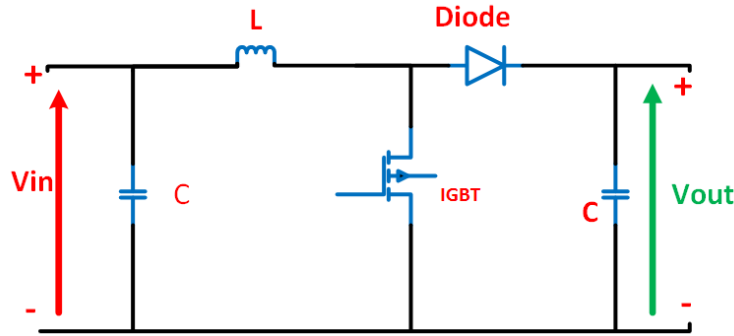


Figure 2. Model of the Boost converter.

The component values of the PV-fed boost converter were designed based on standard engineering practices to ensure stable operation, high efficiency, and a fast dynamic response under the varying conditions imposed by partial shading.

Specifically, the inductor and capacitor values were determined by the following considerations:

The inductance was selected to maintain continuous conduction mode throughout the operating range, thereby reducing current ripple and improving efficiency. The minimum required inductance L_{min} was calculated using [28]:

$$L_{min} = \frac{V_{out} \times (V_{in} - V_{out})}{\Delta I_L \times f_s \times V_{in}} \quad (5)$$

where V_{out} is the PV array voltage, V_{in} is the output voltage, ΔI_L is the desired peak-to-peak inductor current ripple (set to approximately 25% of the average input current), and f_s is the switching frequency.

The output capacitor was sized to limit the output voltage ripple to within 1–2% of v_o . The required capacitance was calculated using [29]:

$$C = \frac{I_{in} \times D}{\Delta V_{in} \times f_s} \quad (6)$$

where I_{in} is the output current, D is the duty cycle, and ΔV_{in} is the allowable voltage ripple.

Based on these calculations and considering practical component availability and system dynamic requirements, the final component values were determined and used in the simulations in.

5. Optimal Power Generation

The Maximum power Point tracking algorithm is an optimization technique that extracts the maximum power generated by a given signal. In this work, the technique is based on a modified P&O model with the flowchart shown in Figure 3

and Figure 4.

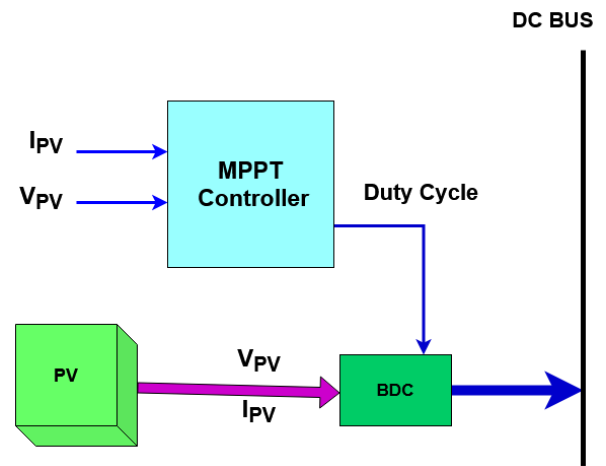


Figure 3. Flowchart of MPPT algorithm using PV generator.

An illustration of MPPT chopper control is shown in Figure 3. The inputs to the control system are the photo current generated and the voltage delivered at the output of the solar panel. DC current shaping produces the required chopper output voltage, which is injected from a DC bus. The use of the boost chopper lies in the fact that it's simple to implement, and the MPPT control enables the output voltage level to be raised. At the DC bus level, it's easy to store energy in battery banks in the form of continuous energy. DC loads can be supplied directly from the DC bus, while AC loads must be supplied via a DC/AC converter.

The scheduling flowchart is shown in Figure 4, which illustrates the various steps involved in extracting maximum power using the observed perturbation algorithms. These algorithms not only determine the size of the overall system, but also enable the voltage level to be adapted in the event of sudden loading of the solar panels or unexpected behavior on the solar system.

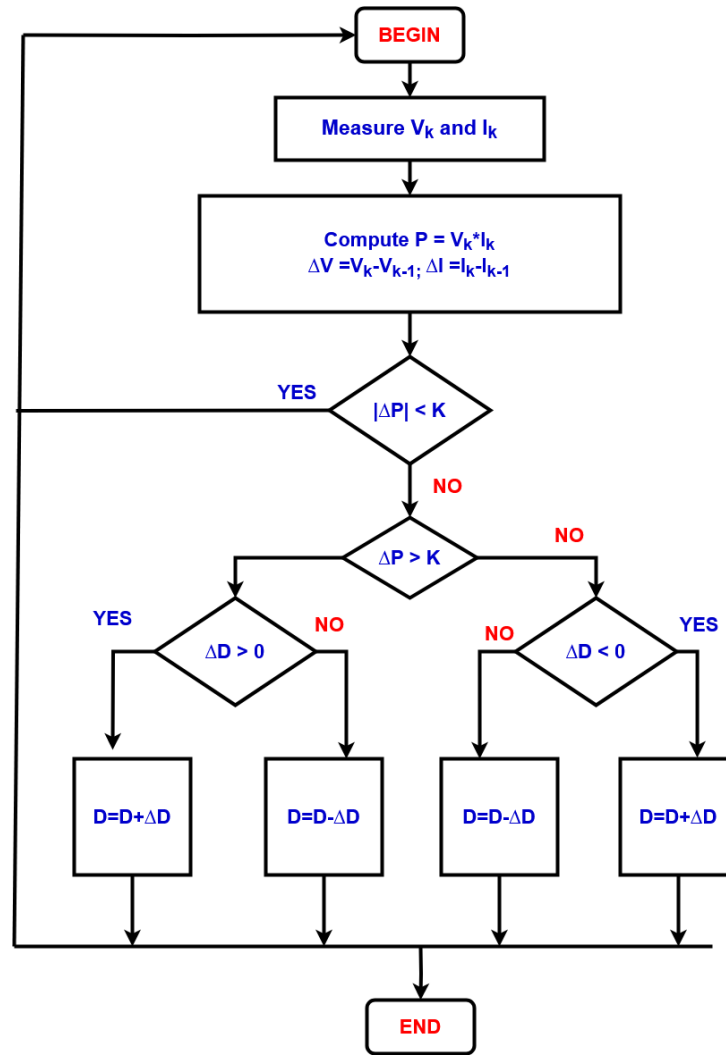


Figure 4. Flowchart of the perturb and observe PV Algorithm.

This technique allows the current generated by the photovoltaic generators to maintain the upper extremum.

6. Topology and Configuration of the System

The overall system configuration is shown in Figure 5. This configuration highlights the photovoltaic solar source, which receives irradiance and temperature as inputs, the essential parameters for producing solar-generated electricity. By varying irradiance and temperature, we obtain voltage-current, voltage-power and current-power characteristics. Extraction of maximum power is achieved by using a DC boost converter. This chopper is controlled by its duty cycle using Maximum Power Point Tracking (MPPT) control. The algorithm determines the duty cycle required for output voltage shaping and maximum extraction of photovoltaic power. From a DC bus, a battery bank is connected to store energy during steady-state operation. Continuous loads can be connected from the DC

bus. For AC loads, a DC/AC converter is required upstream. This inverter generates an output voltage that can be shaped using the proposed active filter.

In addition to smoothing the current and extracting harmonics generated by non-linear loads, filters improve the quality of the DC source from the photovoltaic generator. The importance of the filters is to reduce the rate of harmonic distortion, which will be evaluated in the results section. The system configuration allows other primary DC sources to be connected to the DC bus, but AC sources can be connected from an AC bus after the active filter output. The energy produced by the entire photovoltaic system is fed into the power grids via a step-up transformer, whose output is tapped for voltage and current profiles. The type of transformer depends on the input or primary current source. When the network voltage level is higher than the primary source, a step-up transformer is chosen, whereas when the network voltage level is lower than the source, the step-down transformer is also used to shape the voltage level.

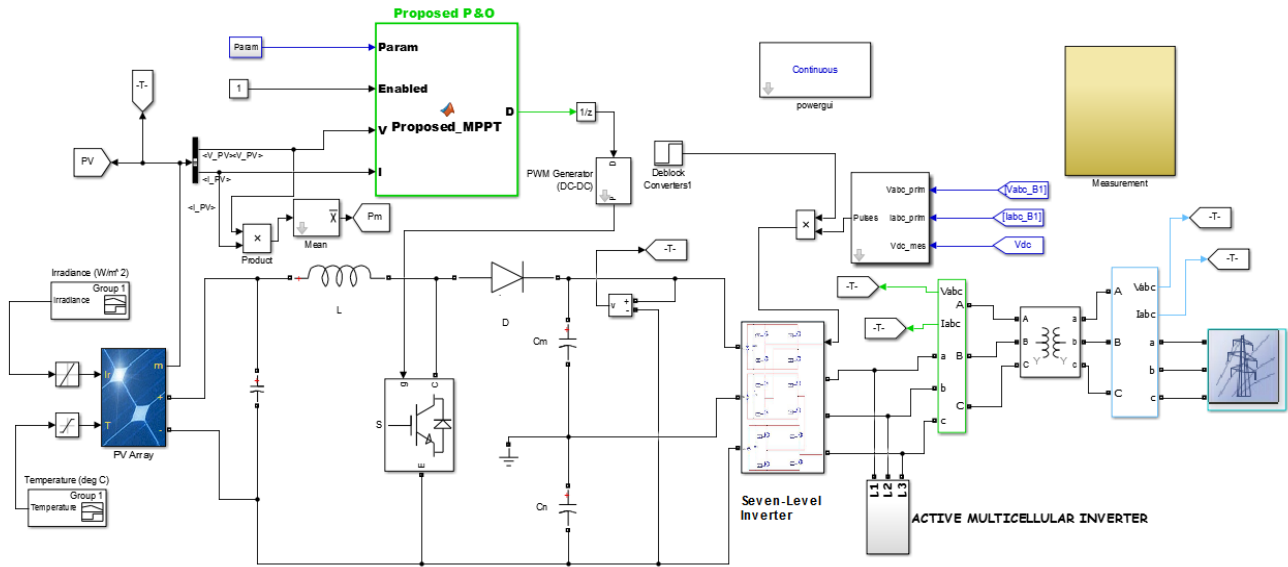


Figure 5. Configuration of overall system.

7. Impact of Photovoltaic System's Characteristics

We carried out a simulation where we maintained constant irradiance ($G = 1000 \text{ W/m}^2$) for different temperatures (from 10°C to 60°C), then different irradiances as also set from $G = 800 \text{ W/m}^2$ to $G = 1000 \text{ W/m}^2$, firstly based on the mathematical equation [7] below, then we varied these parameters.

$$I_s = I_{pho} - I_0 \left[\exp \left(\frac{(V_s + R_s I_s)}{V_T A} \right) - 1 \right] - \frac{V_s + R_s I_s}{R_p} \quad (7)$$

$$I_s = I_{pho} - I_0 \left[\exp \left(\frac{q(V_s + R_s I_s)}{KTA} \right) - 1 \right] - \frac{V_s + R_s I_s}{R_p} \quad (8)$$

$$\text{Where } V_T = \frac{KT}{q}$$

$$I_{pho} = \left[I_{SC} + K_i (T - T_{ref}) \right] \frac{G}{G_n} \quad (9)$$

$$I_0 = I_{n,0} \left(\frac{T_{ref}^3}{T} \right) \exp \left[\frac{qE_g}{AK} \left(\frac{1}{T_{ref}} - \frac{1}{T} \right) \right] \quad (10)$$

In Eq(7), the thermal voltage of the PV cell is V_T ; I_{pho} is the Photo current generated due to incident solar irradiance; The reverse saturation current of the diode is represented by I_0 . The Boltzmann's constant is $K = 1.3806503 \times 10^{-23} \text{ J/K}$. T is the Cell operating temperature in kelvin (K); $q = 1.60217646 \times 10^{-19} \text{ C}$ represents the Charge of the electron; R_s is the Series resistance representing an internal resistance of the PV cell (Ω). The parameter R_p is the Shunt resistance representing the leakage current of the PV cell (Ω); here the parameter A is the Diode ideality factor; I_{sc} is the shunt circuit current of the cell at 25°C and $1,000 \text{ W/m}^2$; K_i is the temperature coefficient of the cell at I_{sc} . T_{ref} represents the reference temperature of the cell; and G is the Solar irradiation (W/m^2). G_n the nominal solar irradiance; $I_{n,0}$ is the nominal saturation current and E_g represents the semiconductor energy band gap which is equal to $E_g = 1.12 \text{ eV}$, considering the polycrystalline silicon cell at 25°C . The Panels characteristics are given in Table 1.

Table 1. Panels characteristics.

Parameters	Monocrystalline	Polycrystalline
Maximum power (W)	50	50
Maximum power voltage (V)	18	18
Maximum power current (A)	2.78	2.77

Parameters	Monocrystalline	Polycrystalline
Open circuit voltage (V)	21.6	19.2
Short circuit current (A)	2.9	3
Number of cells	36	36
Tolerance	$\pm 3\%$	/

7.1. Influence of the Temperature

For an irradiance set at 1000W/m^2 , the temperature was varied from 10 degrees Celsius to 60 degrees Celsius to see the behavior of the power produced by the solar cell as a function of the photo current generated. The curve profiles defined by the maximum power point tracking command

show that when temperature rises, the photo current generated is decreases, in the other hand, at an average of 25 degrees Celsius, the maximum is extracted. Figure 6 shows how, when the temperature moves away from 55 degrees Celsius, power decreases. the curve described by the MPPT function has a good power profile and remains constant for a current at 11.7A and a power that is extracted at 50W.

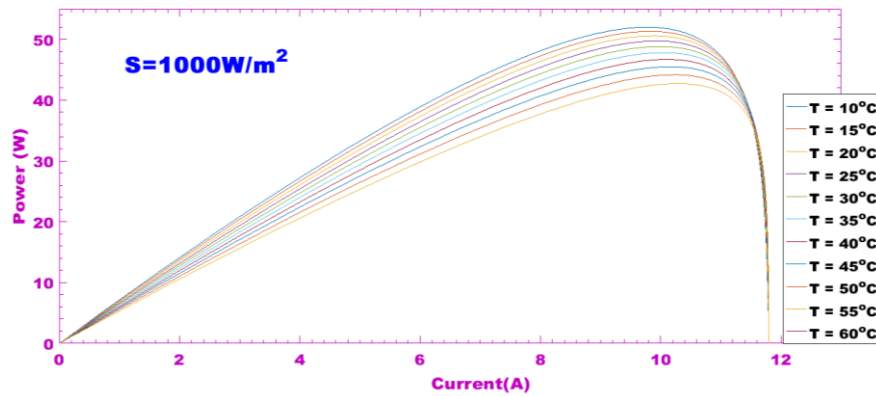


Figure 6. Current/power functions under the influence of temperature.

Figure 7 depicts the variation in power as a function of the voltage produced by the solar cell for irradiance maintained at 1000W/m^2 . For a temperature variation from 10 degrees to 60 degrees, the shape of the functions defined by the MPPT

control shows that power remains almost constant. For a voltage variation up to 7.2V, the power profiles show that maximum power is extracted at 50W for a voltage value of 5.5V and a temperature of 25.4 degrees Celsius.

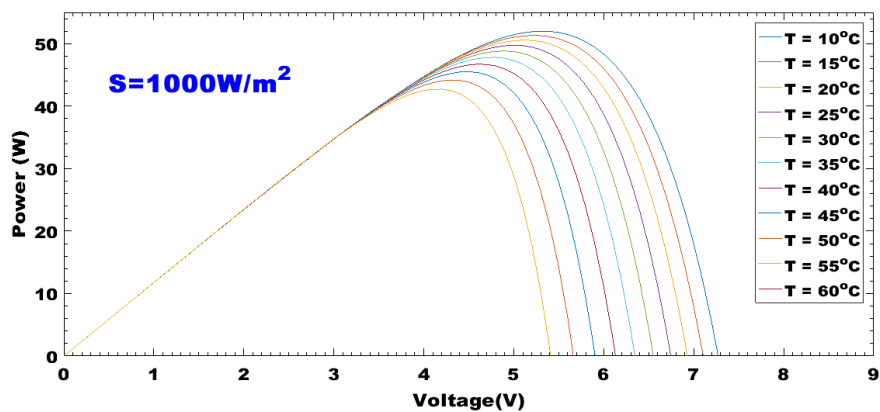


Figure 7. Voltage/power functions under the influence of temperature.

The temperature is always varied from 10 to 60 degrees and irradiance is maintained at 1000W/m^2 . The functions defined by the MPPT command depicts in Figure 8 that the current

remains constant at 12A, for a voltage variation ranging from 1.5V to 7.2V. We can see that as the temperature rises; the photo current generated is reduced.

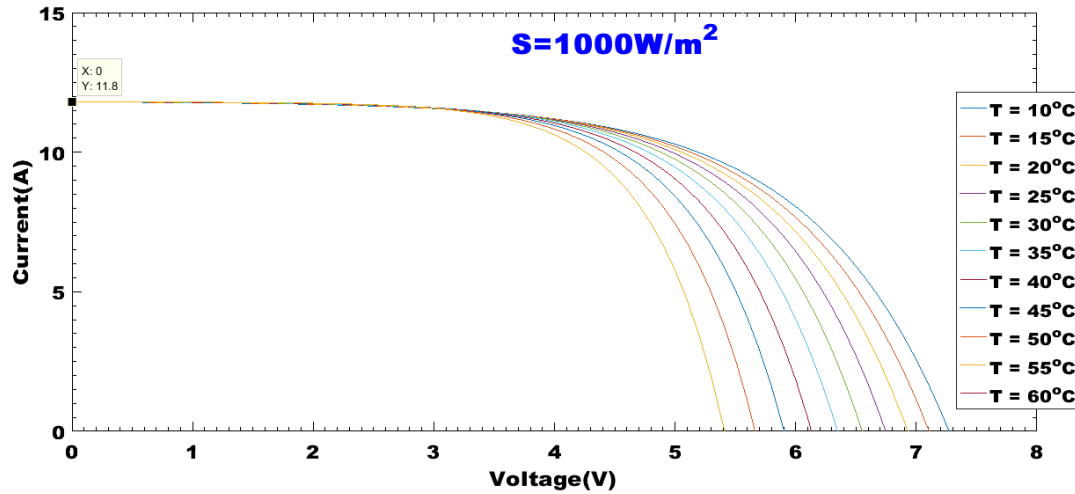


Figure 8. Voltage /current functions under the influence of temperature.

7.2. Influence of the Irradiance

Figure 9 shows the current and power characteristics for a temperature maintained at 25 degrees Celsius and a variation in irradiance ranging from 80W/m^2 to 1300W/m^2 . The Far

North of Cameroon is a Sahelian region with irradiance varying up to 1300W/m^2 and temperatures sometimes exceeding 75 degrees Celsius. The shape of the curve shows that when irradiance increases, power is always kept constant, reaching a maximum point for current values equal to 15.8A and a power of 400.50W.

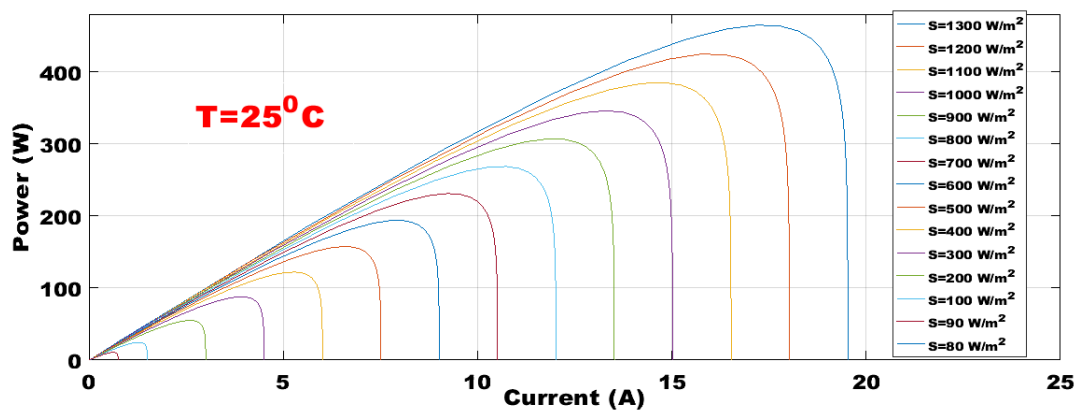


Figure 9. Current/power functions under the influence of irradiance.

Figure 10 shows the power profile defined by the MPPT control for voltages ranging from 0.6 to 34 V. With the temperature maintained at 25 degrees Celsius, the voltage-power

characteristics show good control performance. Maximum power is obtained at 400.99 W for a maximum voltage of 27 V, and an irradiance equivalent to 1200W/m^2 .

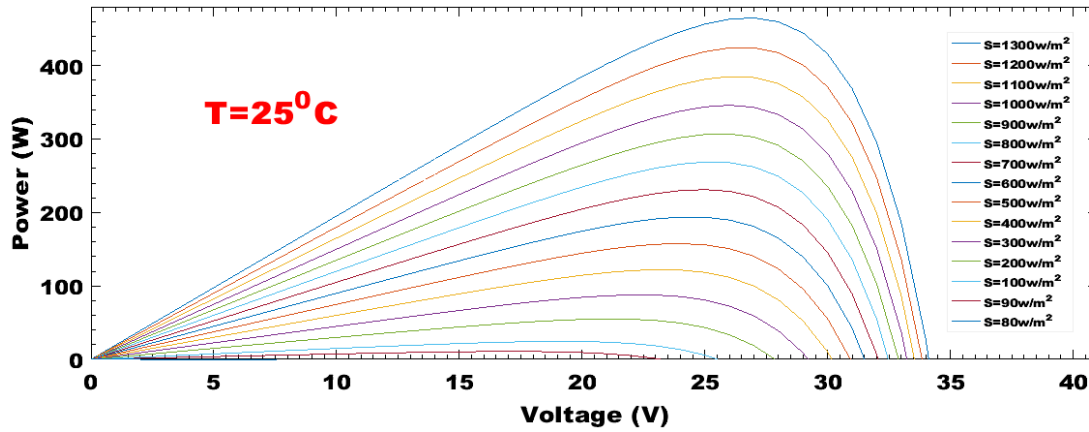


Figure 10. Voltage/power functions under the influence of irradiance.

Figure 11 depicts the voltage-current characteristics of the solar cell when the temperature is maintained at 25 degrees Celsius. Voltages vary up to 34V. Irradiance values range

from 80 m² to 1300W/m². For a variation in irradiance of around 1000W/m², the maximum current is reached at 19.9 A.

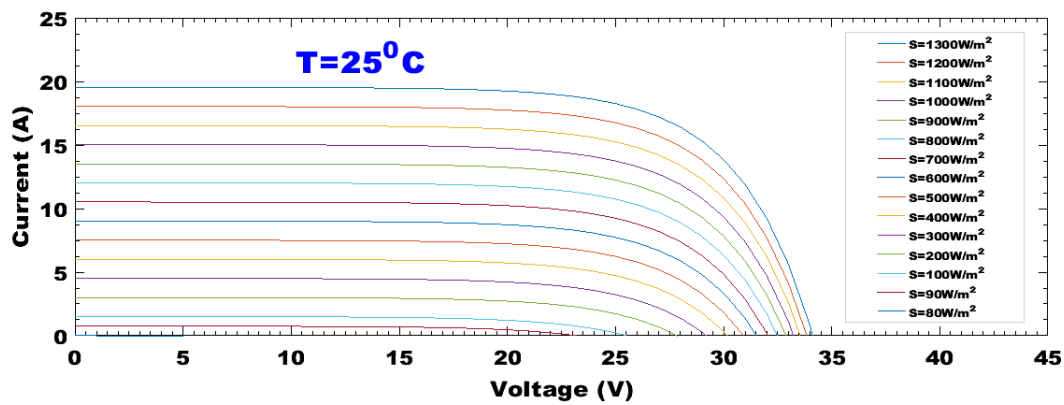


Figure 11. Voltage/current functions under the influence of irradiance.

7.3. Output Currents Profiles Before Filtering

The current profile generated after harmonic distortion is

depicted in Figure 12. These distortions are caused by harmonic currents. It is this disturbance that influences the nature of the inverter's output voltage.

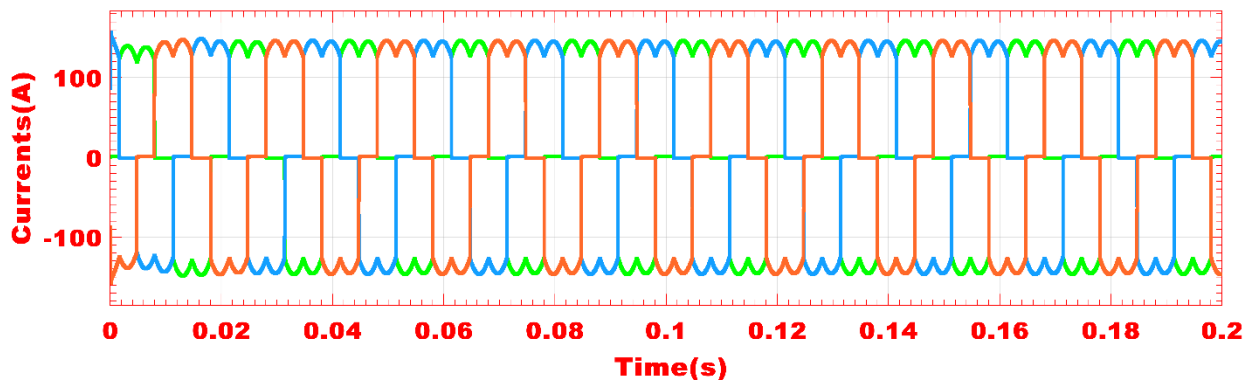


Figure 12. Current waveform deformation due to harmonics.

7.4. Power Compensation

Figure 13 depicts the currents injected by the multicell filter in response to harmonic behavior. By injecting these currents

in response to deformation, the nature of the inverter output voltage is improved. This technique is also used for active power compensation using anti-bounce filters.

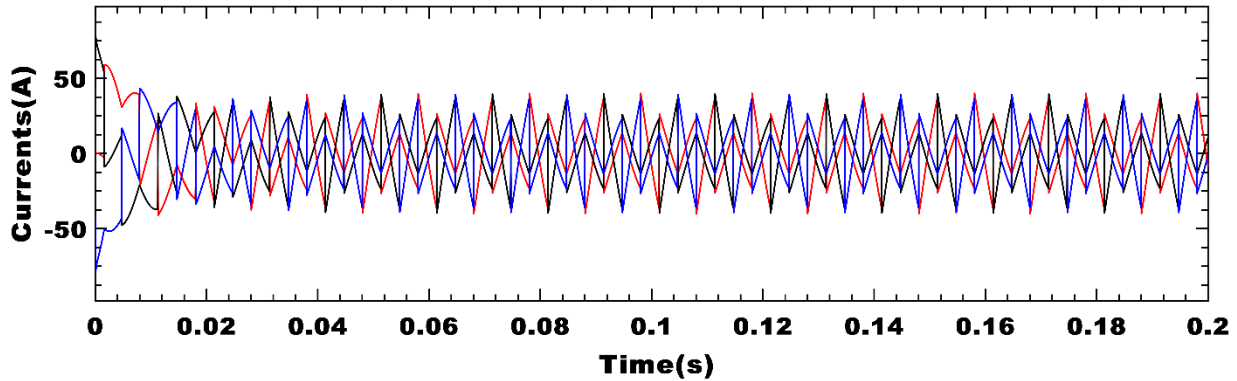


Figure 13. Reference current of the filter to be injected in the Network.

7.5. Harmonic Mitigation

With the PLL synchronization and active filter, the current profiles are shown in Figure 14, which shows a synchronization with reduced delay, thus optimizing active power. The behavior of electrical networks is defined by the simple figure. It can be seen that the currents of the three network phases have good waveforms close to the sinusoid. The evaluation of the harmonic dissolution rate is shown in Figure 14. Calculating the harmonic distortion ratio (THD) enables us to assess the quantity of harmonics injected at a common coupling point. This rate must comply with the IEEE 519-2024 standard. Some recent work [30], advises the calculation of harmonic distortion rates and grid voltage and current profiles when a primary source is injected. Of course, most primary sources, such as wind generators or biomass power plants, have a high level of harmonic distortion. There are also non-linear loads that are a source of harmonic abundance in the distribution or generation network.

lating the harmonic distortion ratio (THD) enables us to assess the quantity of harmonics injected at a common coupling point. This rate must comply with the IEEE 519-2024 standard. Some recent work [30], advises the calculation of harmonic distortion rates and grid voltage and current profiles when a primary source is injected. Of course, most primary sources, such as wind generators or biomass power plants, have a high level of harmonic distortion. There are also non-linear loads that are a source of harmonic abundance in the distribution or generation network.

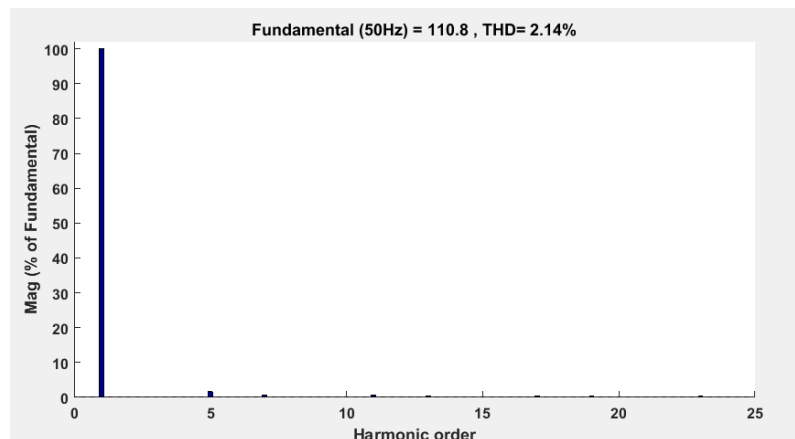


Figure 14. Evaluation of total harmonic distortion.

7.6. Inverter Voltages Profiles

The aim in this work is to provide considerable energy according to household demand for a given locality. A thorough study is required, together with an appropriate choice of

algorithm, so that a techno-economic study can be carried out using software such as Homer Pro. In recent [31] works, it is advisable to carry out a technical-economic study before implementing distributed generators. And in other [32] works, we prefer to use PVSyst to evaluate losses on choppers and inverters. The work presented in Figure 15 shows the impact

of the photovoltaic source on proprietary grids. It can be seen that the impact of the photovoltaic source on the power grid contributes to continuity of service thanks to battery banks. These batteries also help to maintain voltage stability in distribution networks in order to correct load shedding.

The proposed system is designed to generate power for injection into the distribution grid. Figure 15 shows the voltage and current profiles at the output of the three-phase inverter. It can be seen that, after connection to the grid, the waveforms are close to sinusoidal and exhibit radial patterns.

The voltages of the three phases are offset from each other by $2\pi/3$. We can also see that the voltage levels of the three phases are more than sufficient to be injected into power grids.

The voltage range is in the 480V range. As for the voltage and current profile, the waveforms are equally good. Not only are they close to the sinusoid, but they are also within an acceptable range. Inverter output voltages and currents are not rich in harmonics. These signals are shaped by the active filter located at the output of the three-phase inverters.

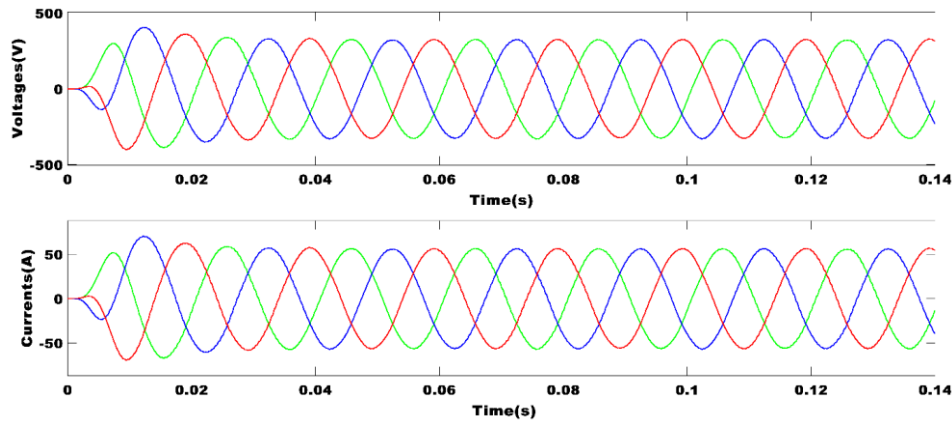


Figure 15. Inverter output characteristics.

The behaviors of currents and voltages are also depicted in Figure 15. These profiles are obtained after synchronization of the proposed system with the power grid. After hooking up the system and synchronizing the frequency of the proposed system with that of the power grid, it can be seen that the use of a step-up transformer is important because the grid voltage level is very high compared to the three-phase voltage levels of the primary source. We observe a slight current whose disturbances are damped within a very short interval. And it also shows how voltages comply with the standard, since high-voltage currents are low, while low-voltage currents are high. This is why we recommend always using the trans-

former when connecting generators distributed on proprietary networks. The harmonic distortion rate obtained in Figure 14 also shows the correct current and voltage waveforms at the output of three-phase inverters.

And the use of PLL synchronization has also ensured the stability and regulation of inverter output voltages. It can be seen that the photovoltaic generator does not have too much of a negative impact on power grids. However, for a short time ranging from 0 to 0.01s, there is a disturbance. This is due to the PLL synchronization and modulation process. This is because regulation by the PI controller is sometimes delayed when the signal shaping system is not properly dimensioned.

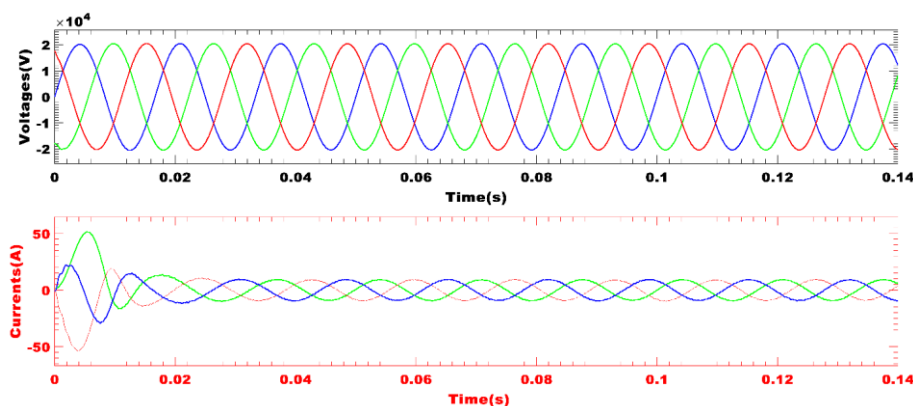


Figure 16. Grid output characteristics.

8. Conclusion

The steps in the method proposed in this article have enabled us, thanks to the MPPT control and the active filter, to gain insight into the behavior of the photovoltaic source, as well as the power quality produced by the proposed system. we note that a harmonic distortion rate of 2.14% is determined after filter threading. This harmonic distortion value complies with the IEEE 519 -2014 standard. The filters have demonstrated their performance, and the perturbed and observed algorithms have enabled the control of the adaptation stage for direct current from photovoltaic generators. In the future, the harmonic distortion rate for such a proposed system will be evaluated, but taking into account sudden changes in irradiance and solar cell shading. Because sudden changes in insolation or the effect of temperature on solar cells should not be overlooked. They can have an impact on the quality of photovoltaic energy on the one hand, and at the same time on the distribution networks into which this photovoltaic source is fed. Feasibility and technico-economic studies can also help to make a conjecture or decision on the injection of this source into a power grid.

Abbreviations

THD	Total Harmonic Distortion
MPPT	Maximum Power Point Tracking
PVG	Photovoltaic Generators
IEEE	Institute of Electrical and Electronics Engineers
P&O	Perturb and Observe
PWM	Pulse Width Modulation
PLL	Phase-locked Loop

Conflicts of Interest

The authors declare no conflicts of interest.

References

- [1] N. Premkumar, M. R. Madhavi, K. Kitmo, and S. Shanmugan, "Utilizing the lignocellulosic fibers from Pineapple Crown Leaves extract for enhancing TiO₂ interfacial bonding in dye-sensitized solar cell photoanodes," *Mater. Renew. Sustain. Energy*, vol. 13, no. 1, pp. 13–25, Apr. 2024, <https://doi.org/10.1007/S40243-023-00245-4/FIGURES/13>
- [2] B.-P. Ngoussandou *et al.*, "Optimal Placement and Sizing of Distributed Generations for Power Losses Minimization Using PSO-Based Deep Learning Techniques," *Smart Grid Renew. Energy*, vol. 14, no. 9, pp. 169–181, Oct. 2023, <https://doi.org/10.4236/SGRE.2023.149010>
- [3] S. Alphonse *et al.*, "Optimization PV/Batteries System: Application in Wouro Kessoum Village Ngaoundere Cameroon," *J. Power Energy Eng.*, vol. 9, no. 11, pp. 50–59, Nov. 2021, <https://doi.org/10.4236/JPEE.2021.911003>
- [4] B.-P. Ngoussandou *et al.*, "Optimal energy scheduling method for the North Cameroonian interconnected grid in response to load shedding," *Sustain. Energy Res.* 2023 101, vol. 10, no. 1, pp. 1–25, Sep. 2023, <https://doi.org/10.1186/S40807-023-00084-X>
- [5] K., G. B. TCHAYA, N. Djongyang, S. Alphonse, and D. K. KAOGA, "Optimization of the smart grids connected using an improved P&O MPPT algorithm and parallel active filters," *J. Sol. Energy Res.*, vol. 6, no. 3, pp. 814–828, Jul. 2021, <https://doi.org/10.22059/JSER.2021.320173.1196>
- [6] M. F. Elnaggar *et al.*, "Optimal sizing and power losses reduction of photovoltaic systems using PSO and LCL filters," *PLoS One*, vol. 19, no. 4, p. e0301516, Apr. 2024, <https://doi.org/10.1371/JOURNAL.PONE.0301516>
- [7] R. Palanisamy, M. Singh, R. Ramkumar, S. Usha, T. M. T. Thentral, and Kitmo, "Capacitor voltage unbalance minimization for three-phase five-level diode-clamped inverter using hexagonal hysteresis space vector modulation," *Multiscale Multidiscip. Model. Exp. Des.*, pp. 1–11, Sep. 2023, <https://doi.org/10.1007/S41939-023-00238-W/METRICS>
- [8] S. Usha, T. M. ThamizhThentral, R. Palanisamy, A. Geetha, P. Geetha, and Kitmo, "Mitigation of circulating current and common mode voltage in grid-connected induction motor drive using modified PID-fuzzy controller," *Multiscale Multidiscip. Model. Exp. Des.*, pp. 1–15, Jul. 2023, <https://doi.org/10.1007/S41939-023-00192-7/METRICS>
- [9] Kitmo, R. Djidimbé, D. K. Kidmo, G. B. Tchaya, and N. Djongyang, "Optimization of the power flow of photovoltaic generators in electrical networks by MPPT algorithm and parallel active filters," *Energy Reports*, vol. 7, pp. 491–505, Nov. 2021, <https://doi.org/10.1016/J.EGYR.2021.07.103>
- [10] Kitmo and M. M. Rahman, "Investments in Energy Complexes: Evidence from Tajikistan," pp. 209–219, 2024, https://doi.org/10.1007/978-3-031-51532-3_17
- [11] Yaouba *et al.*, "An Experimental and Case Study on the Evaluation of the Partial Shading Impact on PV Module Performance Operating Under the Sudano-Sahelian Climate of Cameroon," *Front. Energy Res.*, vol. 10, p. 924285, Aug. 2022, <https://doi.org/10.3389/FENRG.2022.924285/BIBTEX>
- [12] Kitmo, G. B. Tchaya, and N. Djongyang, "Optimization of hybrid grid-tie wind solar power system for large-scale energy supply in Cameroon," *Int. J. Energy Environ. Eng.*, pp. 1–13, Nov. 2022, <https://doi.org/10.1007/S40095-022-00548-8/METRICS>
- [13] M. Jaszczur and Q. Hassan, "An optimisation and sizing of photovoltaic system with supercapacitor for improving self-consumption," *Appl. Energy*, vol. 279, p. 115776, Dec. 2020, <https://doi.org/10.1016/j.apenergy.2020.115776>
- [14] M. Ali, H. Kotb, K. M. Aboras, and N. H. Abbasy, "Design of cascaded pi-fractional order PID controller for improving the frequency response of hybrid microgrid system using gorilla troops optimizer," *IEEE Access*, vol. 9, pp. 150715–150732, 2021, <https://doi.org/10.1109/ACCESS.2021.3125317>

- [15] S. N. A. Latif *et al.*, "The Trend and Status of Energy Resources and Greenhouse Gas Emissions in the Malaysia Power Generation Mix," *Energies* 2021, Vol. 14, Page 2200, vol. 14, no. 8, p. 2200, Apr. 2021, <https://doi.org/10.3390/EN14082200>
- [16] Kitmo, G. B. Tchaya, and N. Djongyang, "Optimization of the photovoltaic systems on the North Cameroon interconnected electrical grid," *Int. J. Energy Environ. Eng.* 2021 131, vol. 13, no. 1, pp. 305–317, Oct. 2021, <https://doi.org/10.1007/S40095-021-00427-8>
- [17] M. Awad, M. M. Mahmoud, Z. M. S. Elbarbary, L. M. Ali, S. N. Fahmy, and A. I. Omar, "Design and analysis of photovoltaic/wind operations at MPPT for hydrogen production using a PEM electrolyzer: Towards innovations in green technology," *PLoS One*, vol. 18, no. 7, p. e0287772, Jul. 2023, <https://doi.org/10.1371/JOURNAL.PONE.0287772>
- [18] M. Haris *et al.*, "Genetic algorithm optimization of heliostat field layout for the design of a central receiver solar thermal power plant," *Heliyon*, vol. 9, no. 11, Nov. 2023, <https://doi.org/10.1016/j.heliyon.2023.e21488>
- [19] B. Andre, S. Alphonse, N. N. Stephane, D. Goron, P. A. Duvalier, and K., "Modeling of a photovoltaic drip irrigation system for an offseason crop: case of onion cultivation in PITOA (North Cameroon)," *Int. J. Eng. Technol.*, vol. 13, no. 1, pp. 1–12, Jan. 2024, <https://doi.org/10.14419/5BJS9B29>
- [20] B. Jyothi, P. Bhavana, B. T. Rao, M. Pushkama, Kitmo, and R. Djidimbele, "Implementation of Modified SEPIC Converter for Renewable Energy Built DC Microgrids," *Int. J. Photoenergy*, vol. 2023, 2023, <https://doi.org/10.1155/2023/2620367>
- [21] S. Liu *et al.*, "Integration method of large-scale photovoltaic system in distribution network based on improved multi-objective TLBO algorithm," *Front. Energy Res.*, vol. 11, p. 1322111, Jan. 2023, <https://doi.org/10.3389/FENRG.2023.1322111/BIBTEX>
- [22] K. K. Dieudonne, M. Bajaj, Kitmo, O. Rubanenko, F. Jurado, and S. Kamel, "Hydropower Potential Assessment of Four Selected Sites in the North Interconnected Network of Cameroon," *2022 IEEE Int. Conf. Autom. Congr. Chil. Assoc. Autom. Control Dev. Sustain. Agric. Syst. ICA-ACCA 2022*, 2022, <https://doi.org/10.1109/ICA-ACCA56767.2022.10005948>
- [23] Kitmo, N. B. Pierre, M. Bajaj, K. M. Aboras, and I. Hossain, "New Approach to Fast and Hyperstable State Observers for Stochastic and Complex Systems," *Int. J. Photoenergy*, vol. 2022, 2022, <https://doi.org/10.1155/2022/2433066>
- [24] A. Boussaibo, A. D. Pene, K. A. Boussaibo, A. D. Pene, and K. , "Optimal Sizing and Power Losses Reduction of Photovoltaic Systems Using PVsyst Software," *J. Power Energy Eng.*, vol. 12, no. 7, pp. 23–38, Jul. 2024, <https://doi.org/10.4236/JPEE.2024.127002>
- [25] Y. Meng, Y. Yang, H. Chung, P. H. Lee, and C. Shao, "Enhancing Sustainability and Energy Efficiency in Smart Factories: A Review," *Sustain.* 2018, Vol. 10, Page 4779, vol. 10, no. 12, p. 4779, Dec. 2018, <https://doi.org/10.3390/SU10124779>
- [26] Y. Wang, J. Xu, L. Feng, and C. Wang, "A Novel Hybrid Modular Three-Level Shunt Active Power Filter," *IEEE Trans. Power Electron.*, vol. 33, no. 9, pp. 7591–7600, 2018, <https://doi.org/10.1109/TPEL.2017.2772811>
- [27] on F. C. IEEE Standards Coordinating Committee 21, Institute of Electrical and Electronics Engineers., and IEEE-SA Standards Board., "IEEE recommended practice for utility interface of photovoltaic (PV) systems," p. 25, 2000.
- [28] Institute of Electrical and Electronics Engineers, *IEEE Std 1547-2018 (Revision of IEEE Std 1547-2003) - IEEE Standard for Interconnection and Interoperability of Distributed Energy Resources with Associated Electric Power Systems Interfaces*. 2018. <https://doi.org/10.1109/IEEESTD.2018.8332112>
- [29] H. Xu, K. P. Seng, L. M. Ang, and J. Smith, "Decentralized and Distributed Learning for AIoT: A Comprehensive Review, Emerging Challenges, and Opportunities," *IEEE Access*, vol. 12, pp. 101016–101052, 2024, <https://doi.org/10.1109/ACCESS.2024.3422211>
- [30] Q. N. Trinh and H. H. Lee, "An enhanced grid current compensator for grid-connected distributed generation under nonlinear loads and grid voltage distortions," *IEEE Trans. Ind. Electron.*, vol. 61, no. 12, pp. 6528–6537, 2014, <https://doi.org/10.1109/TIE.2014.2320218>
- [31] M. H. Yabalar and E. Ercelebi, "Hybrid Optimization Based Harmonic Minimization in Three Phase Multilevel Inverter with Reduced Switch Topology," *IEEE Access*, pp. 1–1, May 2024, <https://doi.org/10.1109/ACCESS.2024.3401730>
- [32] M. Dashtdar *et al.*, "Improving the Power Quality of Island Microgrid with Voltage and Frequency Control Based on a Hybrid Genetic Algorithm and PSO," *IEEE Access*, vol. 10, pp. 105352–105365, 2022, <https://doi.org/10.1109/ACCESS.2022.3201819>